Polymer coating/encapsulation of nanoparticles using a supercritical anti-solvent process

Yulu Wang, Rajesh N. Dave, Robert Pfeffer*

New Jersey Center for Engineered Particulates, New Jersey Institute of Technology, Newark, NJ 07102, USA

Abstract

Coating or encapsulation of nanoparticles is a major challenge due to the extremely small size, high surface energy, and high surface area of the nanoparticles. In this paper we describe a new method using supercritical CO_2 as an anti-solvent (SAS) for nanoparticle coating/encapsulation. A model system, using silica nanoparticles as host particles and Eudragit polymer as the coating material, was chosen for this purpose. The SAS process causes a heterogeneous polymer nucleation with the nanoparticles acting as nuclei and a subsequent growth of polymer on the surface of the nanoparticles induced by mass transfer and phase transition. A polymer matrix structure of encapsulated nanoparticles is formed by agglomeration of the coated nanoparticles. Field emission scanning electron microscopy, transmission electron microscopy, electron energy loss spectroscopy and Fourier transform infrared spectroscopy were used to characterize the coated/encapsulated silica nanoparticles.
© 2003 Elsevier B.V. All rights reserved.

Keywords: Nanoparticles; Coating; Encapsulation; Nucleation; Supercritical anti-solvent

1. Introduction

The rapid development of nanotechnology and nanomaterials has led to a need for nanoparticle surface modification for a variety of applications [1–5]. The surface can be tailored to specific physical, optical, electronic, chemical, and biomedical properties by coating a thin film of material on the surface of the nanoparticles. Conventional nanoparticle coating methods include dry and wet approaches. Dry methods include: (a) physical vapor deposition [6], (b) plasma treatment [7,8], (c) chemical vapor deposition [9], and (d) pyrolysis of polymeric or non-polymeric organic materials for in situ precipitation of nanoparticles within a matrix [10]. Wet methods for coating nanoparticles include: (a) sol–gel processes [1,2] and (b) emulsification and solvent evaporation techniques [5,11,12].

The coating or encapsulation of nanoparticles has been found to be of particular interest for the controlled release of drugs, genes, and other bioactive agents. Controlled release systems provide the benefits of protection from rapid degradation, targeting delivery, control of the release rate, and prolonged duration of bioactive agents. Leroux et al. [4] studied the surface modification of nanoparticles of poly D,L-lactic acid (D,L-PLA) loaded with drugs to improve site-specific drug delivery. The drug delivery system was prepared using the emulsion method.

* Corresponding author. Tel./fax: +1-973-642-7496.
  E-mail address: pfeffer@adm.njit.edu (R. Pfeffer).

Results indicated that drug loaded nanoparticles of D,L-PLA, which were coated with poly ethylene glycol (PEG), provided protection from uptake by human monocytes. The findings revealed that surface modified nanoparticles with PEG could temporarily avoid the mononuclear phagocyte system and substantially prolong the circulation time of the nanoparticles.

Cohen et al. [5] prepared a sustained gene delivery system of DNA encapsulated in polymeric nanoparticles using a double emulsion approach. In their research the gene delivery system was found to offer increased resistance to nuclease degradation since the polymeric coating provides protection from serum nuclease. The activity of plasmid DNA administration was found to be in the sustained duration mode. The gene delivery system is a potential formulation for the application of gene therapy.

The emulsion techniques used above are associated with the following four steps: (a) preparing the solution of polymer and bioactive agent in an organic solvent, (b) dispersing the solution in another phase under vigorous stirring, (c) stabilizing under certain temperature and pH conditions, and (d) evaporating the organic solvent. However, during the emulsion preparation, the organic solvent and the strong shearing force, temperature, pH, and the interface between the oil and water phases may affect and/or alter the structure of the bioactive agents [13–16]. Moreover, some severe drawbacks such as residual organic solvent in the final product, volatile organic compounds emission, and heavy downstream processing are involved in emulsion processes.

The objective of this research is to develop a new technique for coating or encapsulation of ultrafine particles (sub-micron and nanoparticles) to modify their surface properties by using supercritical CO_2 (SC CO_2) in a SAS process. CO_2 is an ideal processing medium because of its relatively mild critical conditions ($T_c = 304.1$ K, $P_c = 7.38$ MPa). Furthermore, carbon dioxide is non-toxic, non-flammable, relatively inexpensive and recyclable.

There are a number of studies dealing with particle coating or encapsulation using SC CO_2. Kim et al. [17] reported the microencapsulation of naproxen using rapid expansion of supercritical solutions (RESS). The RESS process was also used to coat/encapsulate particles by Mishima et al. [18]. In the RESS coating process the material to be coated and the coating ma-

terial (polymer) are both dissolved in SC CO_2 with or without a cosolvent. The solution is then released from a nozzle (de-pressurized), generating microparticles with a polymer coating on the surface. In RESS the rapid de-pressurization of the supercritical solution causes a substantial lowering of the solvent power of CO_2 leading to very high super-saturation of solute, precipitation, nucleation and particle growth. However, the application of the RESS process is severely limited by the fact that polymers, in general, have very limited solubility in SC CO_2 at temperatures below 80 °C [19]. Also, the operating pressure in RESS is usually above 200 bars so that it is less attractive economically.

Tsutsumi et al. [20,21] used a combination of the RESS process and a fluidized bed for coating particles. In their research, a solution of coating material in SC CO_2 rather than in an organic solvent is sprayed into the fluidized bed of particles to be coated. However, particles less than 30–50 μm fall into Geldart's group C particle classification and are very difficult to fluidize. Hence this method cannot be used to coat ultrafine particles.

Pessey et al. [22,23] also demonstrated particle coating using a supercritical fluid process. Their research involved the thermal decomposition of an organic precursor and the deposition of copper onto the surface of core particles in SC CO_2 under conditions of temperature up to 473 K and pressure up to 190 MPa. However, their methods are less attractive from the point of view of safety and cost and probably cannot be applied to the pharmaceutical industry since high temperature could adversely effect or even destroy most drug powders.

The use of SC CO_2 as an anti-solvent (SAS process), however, can usually be performed at a pressure lower than 10 MPa and at a temperature just above the critical temperature (304.1 K). Also the SAS process is quite flexible in terms of solvent choice. Thus the synthesis of ultrafine particles using SAS has been reported in a number of studies [24–27].

Falk et al. [26] investigated the production of composite microsphere by the SAS process. In their research a homogeneous solution of various solutes and polymer was sprayed into SC CO_2 antisolvent. Co-precipitation of the solutes and polymer occurred and composite microspheres or microcapsules were formed. Recently, Young et al. [27] investigated

the encapsulation of lysozyme with a biodegradable polymer by precipitation with a vapor-over-liquid antisolvent, which is a modified precipitation with a compressed anti-solvent process. In their research, the vapor-over-liquid antisolvent coating process was used to encapsulate 1–10 μm lysozyme particles.

The SAS process is based on the principle of SC CO_2 induced phase separation in which the solute precipitates due to a high super-saturation produced by the mutual diffusion of organic solvent into SC CO_2 and vice versa when an organic liquid solution comes into contact with SC CO_2. An important feature of the SAS process is that the organic solvent can be almost completely removed by simply flushing with pure CO_2. Thus, dry particles are produced after a CO_2 extraction step (flushing) following feeding of the organic solution [28].

2. Experimental

2.1. Materials

To evaluate the efficiency of the SC CO_2 SAS coating process, both hydrophobic and hydrophilic silica nanoparticles of different sizes (Table 1) from Degussa, USA and Catalysts & Chemicals Ind. Co., Japan were chosen as host particles. Eudragit® RL 100 (Rohm America LLC, USA), a copolymer of acrylate and methacrylate, with an average molecular weight of 150 000, was chosen as the coating material. The chemical structure of Eudragit® RL 100 is shown in Fig. 1. Bone-dry grade liquid CO_2 was supplied by Matheson Gas, USA. HPLC grade acetone was purchased from Fisher, USA. All of the materials were used as received without further treatment.

2.2. Methods

The experimental set-up, schematically shown in Fig. 2, consists of a CO_2 supply system, a solution
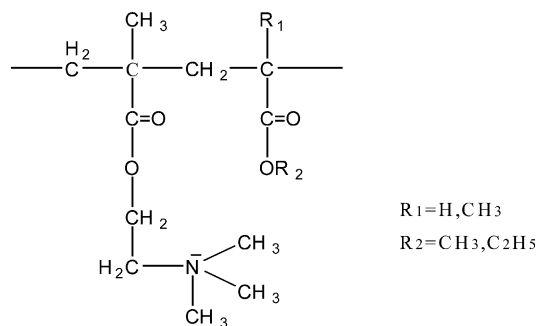

$R_1 = H, CH_3$
$R_2 = CH_3, C_2H_5$

Fig. 1. Chemical structure of Eudragit®.

delivery system, and a high-pressure vessel (Parr Instruments, USA) having a capacity of 1 l. The high-pressure vessel is immersed in a water-bath to keep the temperature constant during an experiment. A metering pump (Model EL-1A, AMERICAN LEWA®, USA) was used to deliver liquefied CO_2 from a CO_2 cylinder to the high-pressure vessel. However, before entering the pump head the liquefied CO_2 was cooled down to around zero degrees Centigrade by using a refrigerator (NESLAB, RTE-111) to minimize cavitation. After leaving the pump head, liquefied CO_2 was pre-heated using a heating tape (Berstead Thermolyne, BIH 171-100).

A polymer solution was prepared by dissolving Eudragit in acetone. Silica nanoparticles were suspended in the polymer solution to produce the desired ratio of polymer to silica particles by weight. Since the 600 nm silica particles possess less surface area than 16–20 nm silica, less polymer is required to coat the 600 nm silica nanoparticles. Therefore, 14–20% by weight of polymer was used for coating the 600-nm silica as compared with 33–50% for coating the 16–20 nm silica. An ultrasonicator was used to break up the nanoparticle agglomerates in the silica–acetone suspension. During the experiments the temperature and pressure were kept at 305.5 K and 8.27 MPa, respectively. When steady state conditions were reached in the high-pressure vessel, i.e., the pressure and

Table 1
Silica nanoparticles used in the experiments

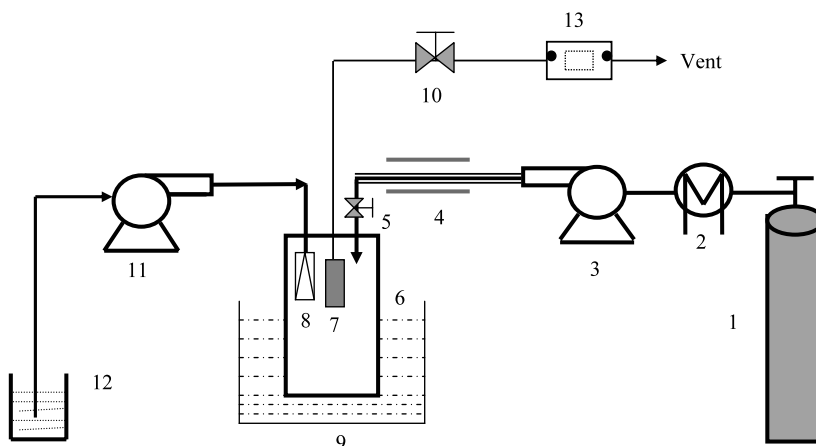| Suppliers	Catalysts & Chemicals Ind. Co. (Japan)	Degussa (USA)	
Trade name	COSMO 55	Aerosil® 90	Aerosil® R 972
Particle size (nm)	600	20	16
Surface property	Hydrophilic	Hydrophilic	Hydrophobic

Fig. 2. Schematic Diagram of Nanoparticle Coating Process Using SAS.

temperature of the CO_2 became stable, the suspension was delivered by a high-pressure pump (Beckman, 110B) at a rate of 0.7 ml/min and was sprayed through a stainless steel capilliary nozzle (125 μm ID) into the high-pressure vessel. The spraying lasted about 20 min followed by another 30 min for settling. Thereafter, CO_2 was supplied at a rate of less than 3.0 standard l/min to remove any residual organic solvent. The cleaning step continued for about 3 h (e.g. at a CO_2 flow rate of 1.8 standard l/min) depending on the CO_2 flow rate and the temperature. The higher the flushing velocity and higher the temperature, the less flushing time is required. When the cleaning step was completed, the high-pressure vessel was slowly depressurized and samples were collected for characterization. The experimental parameters are given in Table 2.

Table 2
Experimental parameters in SAS coating process

Experiments	Parameters	
	Polymer concentration (g/100 ml)	Ratio of polymer to nanoparticles (g/g)
Coating of 16 nm hydrophobic silica	0.8	1:2
Coating of 20 nm hydrophilic silica	0.8	1:1
Coating of 600 nm hydrophilic silica	0.4	1:4
		1:5
		1:6

3. Characterization

In this study it is necessary to use a high-resolution field emission scanning electron microscope (FE-SEM) (Jeol, JSM-6700F) for morphological observations since the primary particles are less than 100 nm. Specimens were sputter coated with palladium (SPI Sputter) for 20 s to make the surface conductive without compromising fine surface microstructure. A nonconductive surface would produce a severe surface charge problem under the high intensity electron beam and accumulated surface charge would cause abnormal contrast, image deformation and distortion. A Leo 922 Omega Transmission Electron Microscope (TEM) was also used to examine the structure of the encapsulated nanoparticles.

Fourier Transform-Infrared (FT-IR) spectroscopy measurements were carried out using a Spectrum One FT-IR Spectrometer (PerkinElmer Instruments) with PerkElmer V3.02 Software Spectrum for control of the instrument, data acquisition and analysis. The spectra were taken in the range of 400–4000/cm using a resolution of 8/cm and 25 scans. The spectra of the polymer, uncoated and coated silica nanoparticles were measured as pellets. The pellets of uncoated and coated silica nanoparticles were made by mixing them with ground KBr at a ratio of 0.85% (w/w) and were pressed by a press kit (International Crystal Laboratories) and a 12-ton hydraulic Carver Laboratory Press (Fred S. Carver Inc.). KBr has no absorbance in the IR range, and served as a diluent for the solid

samples. In preparing the polymer specimen, Eudragit pellets were ground into powder using a mortar and pestle. The ground Eudragit was then mixed with ground KBr at a ratio of 0.5% (w/w). Afterward, the mixture was made into a pellet for characterization.

4. Results and discussion

4.1. Fundamentals of the SAS process

In the SAS process, SC CO_2 acts as an anti-solvent, which is dissolved in the organic solvent, reducing the solvent strength significantly [29] leading to a high degree of super-saturation and nucleation of the solute. While the actual SAS process is complicated due to the interplay of thermodynamics, mass transfer, and hydrodynamic effects [25], a schematic phase diagram of SC CO_2, solvent and solute at constant temperature and pressure is useful to understand the SAS process and is shown in Fig. 3. In this example, SC CO_2 is completely miscible with the solvent, while the polymer and SC CO_2 are partially miscible. The solubility of polymer in SC CO_2 is very limited. Generally, almost all polymers have very low solubility even at 323 K and 30 MPa [25]. In this diagram, the one-phase region $\Phi1$ represents the polymer dissolved in solvent, forming a polymer solution with some CO_2 dissolved in the solution. Region $\Phi2$ is glassy region, a polymer-rich phase, with a small amount of CO_2 and solvent absorbed in the polymer. In the two-phase region, solvent-rich phase $\Phi1$ and polymer-rich phase $\Phi2$ coexist and are in equilibrium.
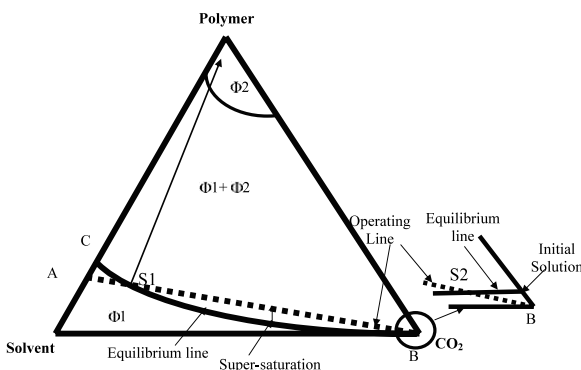

Fig. 3. Typical ternary phase diagram for solvent–polymer–CO_2 at constant *P* and *T*.

The bold line (from C to B, Fig. 3) represents the polymer solubility in the mixture of solvent and SC CO_2. The dotted straight line is an operating line that represents the addition of polymer solution into SC CO_2 (from B to A). During the addition of polymer solution into SC CO_2, an initial very small amount of solute will be dissolved in SC CO_2 with the solvent acting as co-solvent ($\Phi1$ region) until the saturation of polymer in the mixture of SC CO_2 and the solvent is reached (S2, saturation point). Continued feeding of the solution into SC CO_2 results in crossing over the equilibrium boundary and super-saturation of the polymer in the mixture of SC CO_2 and solvent. Subsequently, a phase transition will take place, depending on the starting conditions. The phase transition will occur initially either by nucleation, an activated process in which a free energy barrier must be surmounted, or by spinodal decomposition, a spontaneous process in which no free energy barrier must be overcome [30]. In either case nucleation and precipitation of polymer induced by the phase transition will take place on the surface of the nanoparticles, forming a thin layer of polymer coating.

In our study of nanoparticle coating or encapsulation with polymer using the SAS coating process, the polymer solution with suspended nanoparticles is sprayed through a nozzle. If the solvent and the SC CO_2 are completely miscible and the operating conditions are above the critical point of the mixture, distinct droplets will never form as reported by Lengsfeld et al. [31] and Bristow et al. [32] and the polymer will nucleate and grow within the expanding gas plume. However, our experiments were operated at a temperature of 305.5 K and a pressure of 8.27 MPa, which is in the partially miscible region since the mixture's critical point is 310 K and 7.32 MPa. Furthermore, our group has recently published a new experimental paper [33] which shows that a transient jet and jet-induced droplets exist even when the pressure is slightly above the mixture critical pressure. We observed that only when the pressure is somewhat above the mixture critical pressure does the flow behave like a single-phase gaseous jet without any definable interfacial boundaries or the formation of droplets. Therefore, we assume that in our experiments, droplets of polymer solution with entrapped nanoparticles were generated due to jet break-up.

When a droplet contacts the SC CO_2, since acetone is highly miscible with SC CO_2, a very fast mutual diffusion into and out of the droplet occurs. The polymer solution in the droplet approaches saturation very rapidly due to the extraction of solvent from the droplet. The subsequent crossing over the equilibrium boundary initiates the gelation of the polymer. Meanwhile, the SC CO_2 continuously diffuses into the droplet and is dissolved in the acetone solution. This process leads to swelling of the droplet [28].

When the solvent expansion is high, Reverchon [34] proposed that an empty shell or balloon structure is formed due to the interplay of mass transfer and the phase transition. This empty shell structure was clearly observed in experiments using the SC CO_2 SAS process for particle formation (see figure 6 in Ref. [34]). The stability of the balloon structure depends mainly on the expansion of the solvent by SC CO_2, which depends on the miscibility of the solvent and SC CO_2. In this study acetone, which is highly miscible with SC CO_2, was used as the solvent for the polymer. Thus it is highly probable that a balloon structure was formed which then burst into very fine viscous droplets containing nanoparticles and polymer as shown in the cartoon in Fig. 4.

Further extraction of the solvent by SC CO_2 from the gelled droplets containing nanoparticles induced the glass transition of the polymer. Therefore, the nanoparticles were encapsulated within a polymer film attributed to the nucleation and precipitation of polymer on the surface of the nanoparticles. However, the encapsulated nanoparticles within the polymer film were aggregated and agglomeration took place. Thus, a nanocomposite with a matrix structure was formed with the nanoparticles as the host particles and the polymer as a coating.

4.2. Coating of hydrophobic silica nanoparticles

Hydrophobic silica nanoparticles R972 (Table 1) were chosen to evaluate the coating of nanoparticles with a hydrophobic surface. Fig. 5 shows the morphology and size of the hydrophobic silica nanoparticles at two different magnifications. As can be observed, the hydrophobic silica nanoparticles exhibit the typical chained structure. From the scale bar of the higher magnification micrograph the primary particle size is estimated to be about 16–30 nm.

Fig. 6 shows the SEM micrographs of the hydrophobic silica nanoparticles coated with Eudragit at two different magnifications. When compared with Fig. 5, the morphology of the coated nanoparticles is quite different from that of uncoated nanoparticles. Furthermore, the primary particle size of coated hydrophobic silica nanoparticles is found to be increased to 50–100 nm. The morphological change and size enlargement are attributed to polymer nucleation and subsequent growth on the surface of the nanoparticles during the SAS coating process, forming a thin film encapsulation. The thickness of the polymer film is estimated to be around 10–40 nm.
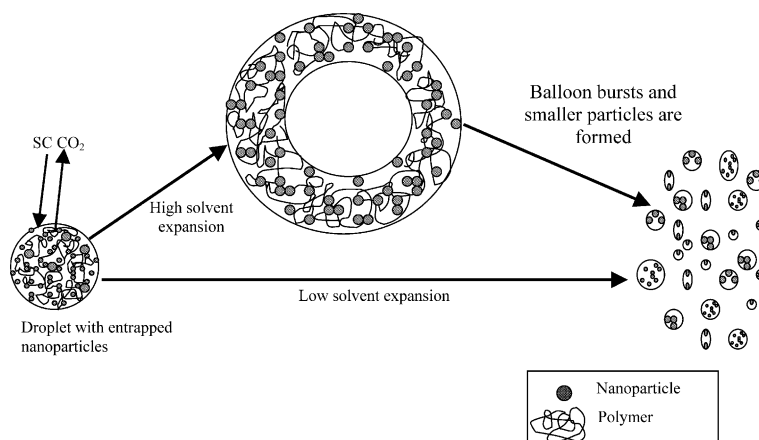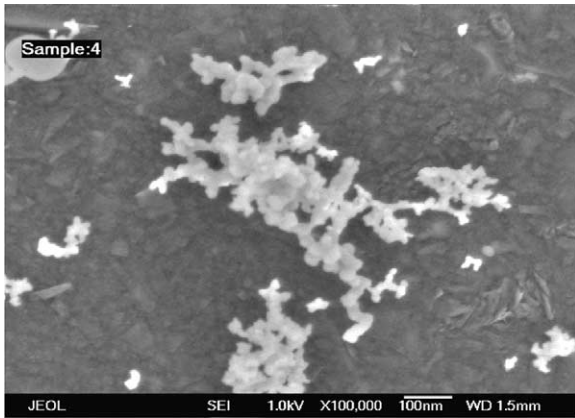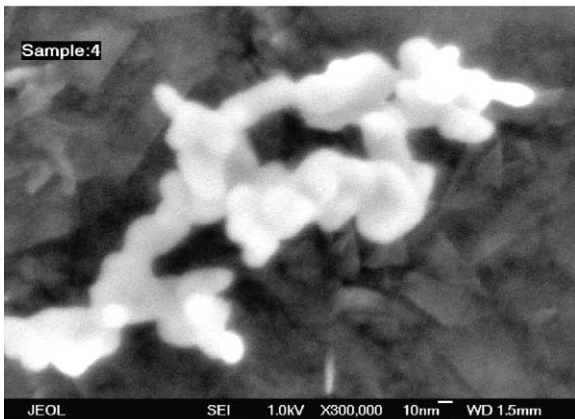

Fig. 4. Possible mechanism of fine particle encapsulation using the SAS process.

(a)

(b)

Fig. 5. SEM micrographs of uncoated hydrophobic silica nanoparticles. (a) × 100 000; (b) ×300 000.

(a)

(b)

Fig. 6. SEM micrographs of hydrophobic silica nanoparticles coated with Eudragit. (a) × 50 000; (b) × 300 000.

TEM-EELS, which is a powerful tool in multi-component material characterization, was used to characterize the encapsulation of the nanoparticles. In TEM-EELS specimen preparation, a wet method was employed to achieve a good dispersion. The encapsulated samples were dispersed in alcohol, and then were spread over an extremely thin carbon film (3 nm) supported by a copper grid. Zero-loss micrographs of uncoated and coated silica nanoparticles are shown in Fig. 7(a) and Fig. 8(a), respectively. Compared with Fig. 7(a), the coated primary particle size (Fig. 8(a)) is estimated to be about 50 nm from the scale bar. The silicon mapping (Fig. 8(b)) exhibits the same shape and morphology of the silica nanoparticle agglomerate as the TEM Zero-Loss micrograph

(Fig. 8(a)). As one of the major components of the polymer, carbon shows up in a carbon mapping micrograph (Fig. 8(c)). The carbon signal is generally weaker than the silicon signal because the amount of carbon is much less than that of silicon. Furthermore, carbon is number six in the periodical table, while silicon is number fourteen, and the higher the atomic number, the stronger the signal response to electrons.

From the carbon mapping, it is clear that the silica nanoparticles are coated with a thin layer of polymer. Interestingly, the coating layer looks like a shell encapsulating the nanoparticle agglomerate. However, from the carbon mapping, it also appears that the polymer is not uniformly distributed on the surface of
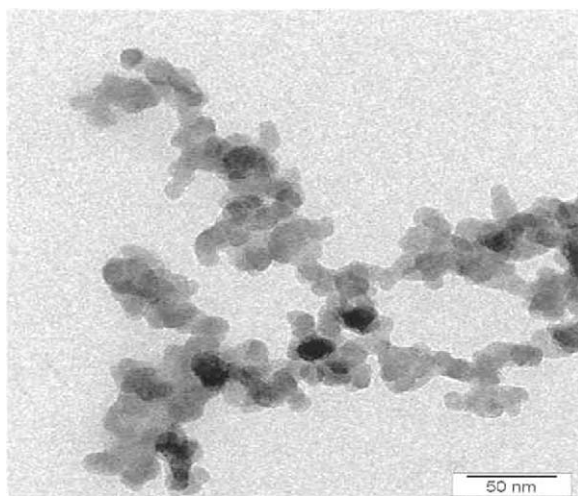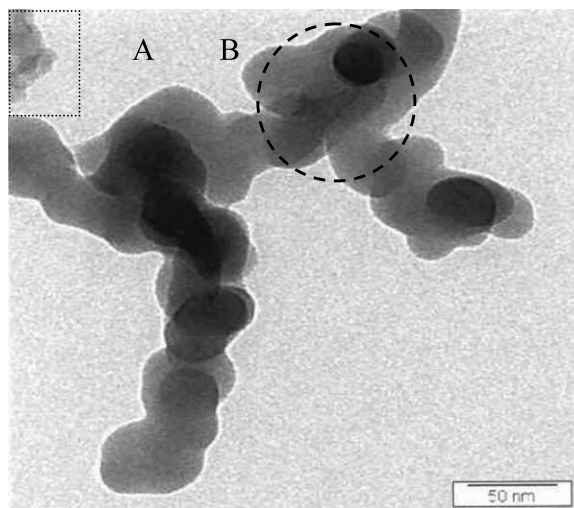
(a)
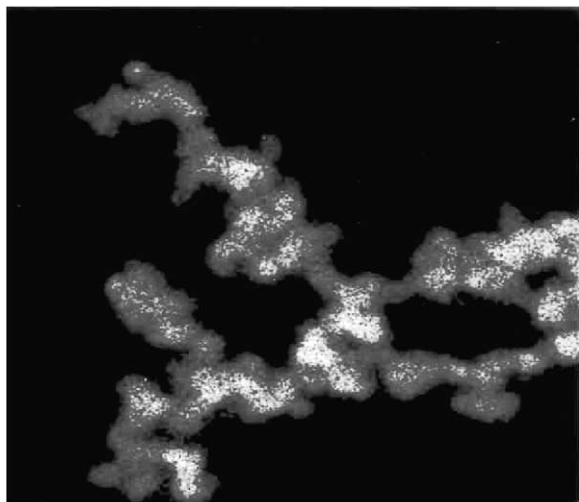
(b)

Fig. 7. TEM-EELS micrographs of uncoated hydrophobic silica nanoparticles. (a) Zero loss; (b) silicon mapping.

the silica nanoparticles. In general, the stronger the carbon signal, the more the polymer has precipitated on the surface of the silica nanoparticles. In region B, it appears that more polymer coating occurs. Another feature in the carbon mapping micrograph is seen at the upper-left corner where an irregular shaped region appears (A in Fig. 8(a)). The corresponding carbon signal is strong (Fig. 8(c)), whereas there is practically no silicon signal in that region (Fig. 8(b)). Therefore,

it can be concluded that the irregular shaped region is heavily coated with polymer.

FT-IR spectrometry is a valuable characterization tool to determine the chemical composition before and after the coating process. Three sets of FT-IR spectra of silica nanoparticles coated with polymer, uncoated silica nanoparticles, and of the Eudragit powder are shown in Fig. 9. The spectrum of Eudragit, which is a copolymer of acrylate and methacrylate, is shown
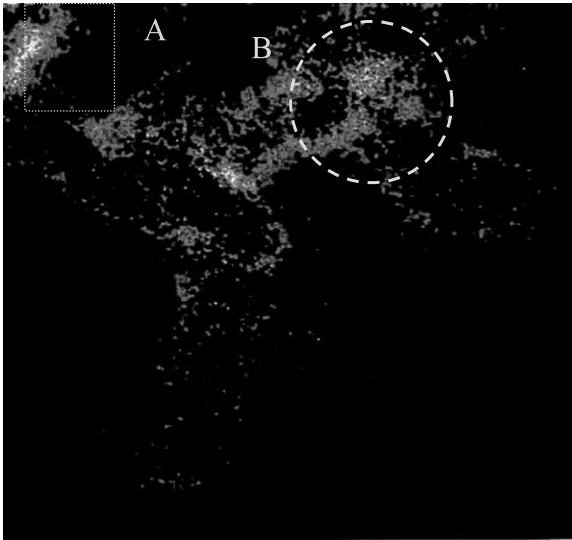

(a)
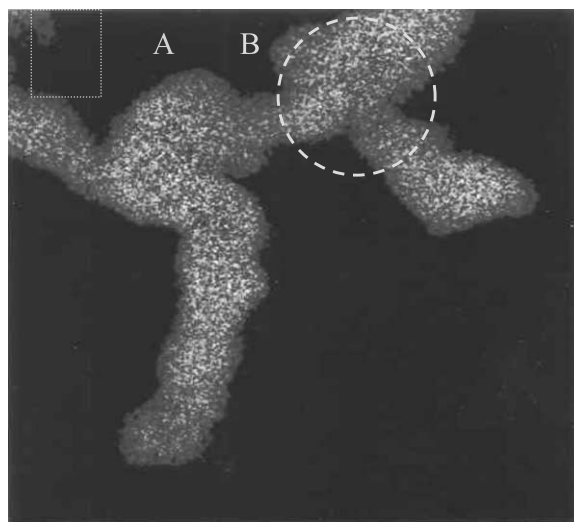
(b)

Fig. 8. TEM-EELS micrographs of coated hydrophobic silica nanoparticles. (a) Zero loss; (b) silicon mapping; (c) carbon mapping.

(c)

Fig. 8. (*Continued*).

in Fig. 9(c). The peaks at 2992.61 and 2954.18/cm are the absorbances of the alkyl groups (–CH$_3$ and –CH$_2$) stretching vibrations. The corresponding absorbances of bending vibrations occur at 1480.47, 1448.6 and 1388.0/cm. A major peak at 1732.27/cm is attributed to the stretching vibration from the car-

bonyl group. The band between 1300 and 1000/cm is assigned to the polymer's C–O double bond stretching mode. The peaks before 1000/cm is the fingerprint region of the polymer. The spectrum of silica nanoparticles in Fig. 9(b) shows a major peak at 1104.38/cm, this is assigned to the Si–O stretching vibration.

When compared with Fig. 9(c), it can be observed in the spectrum of coated silica nanoparticles in Fig. 9(a) that the peaks at 2992.61 and 2954.18/cm associated with alkyl groups' stretching modes and peaks at 1480.47, 1448.6, and 1388.0/cm associated with their bending vibrations show up. At exactly the same position as in the spectrum of polymer, the absorbance at 1732.27/cm assigned to carbonyl group stretching vibration can be found in Fig. 9(a). However, the Si–O stretching vibration and the C–O double bond stretching vibration have almost the same absorbance region from 1300 to 1000/cm. The absorbance of the Si–O stretching mode is much stronger than that of the C–O, hiding the peaks attributed to C–O. Therefore, C–O double bond peaks do not show up in the spectrum of coated silica nanoparticles. From the FT-IR chemical analysis above, a conclusion can be reached that the surface of silica nanoparticles is coated with polymer. This strongly supports the TEM-EELS observations.

However, it is observed that no new peak shows up in the spectrum of silica nanoparticles coated with
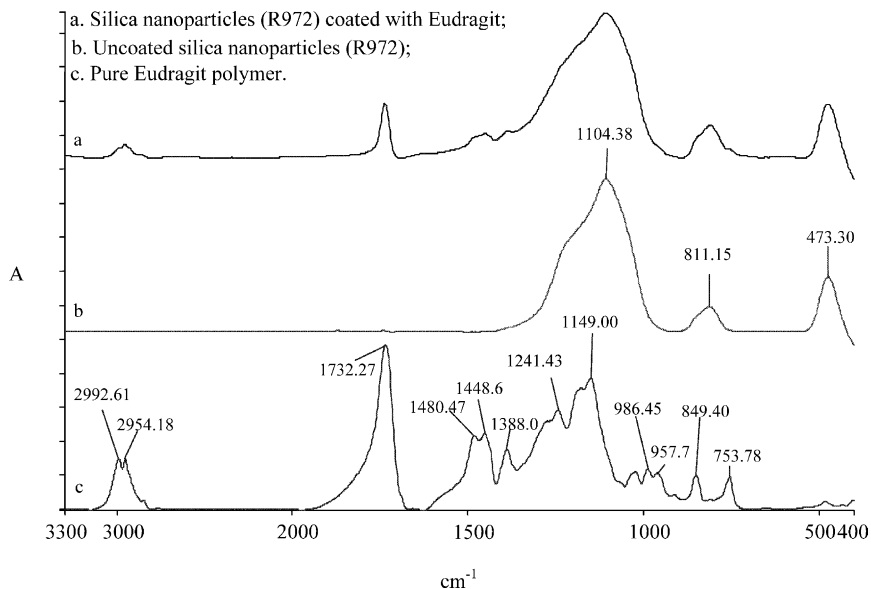

Fig. 9. FT-IR spectra for hydrophobic silica nanoparticles. (a) Coated nanoparticles; (b) uncoated nanoparticles (R972); (c) Eudragit.

Eudragit, indicating that there is no chemical bond between the polymer and the surface of the silica nanoparticles during the process of nanoparticle coating with polymer using the SAS coating process. The SAS coating process is a process of polymer nucleation and subsequent growth on the surface of a particle, typically a physical process. Thus, it is favorable for pharmaceutical applications since any chemical interaction between the coating and the substrate may result in a change in the properties of the pharmaceutical component, which could change the effectiveness of the drug.
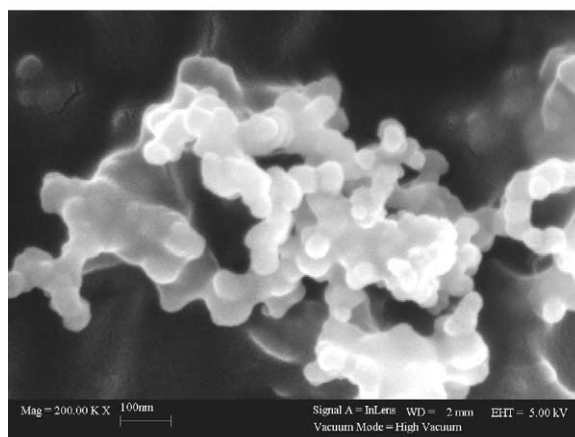
4.3. Coating of hydrophilic silica nanoparticles

Hydrophilic silica nanoparticles (Table 1) were also studied to determine the effect of the hydrophilic surface (if any) on coating with polymer. The uncoated and coated samples were examined using the FE-SEM. Fig. 10 shows micrographs of hydrophilic silica nanoparticles before and after coating. It is clear that a morphological change occurred indicating that the hydrophilic silica nanoparticles were coated with polymer.

The coated hydrophilic silica nanoparticles were also characterized using TEM. The TEM micrographs of hydrophilic silica nanoparticles before and after SAS coating can be seen in Fig. 11(a) and (b), respectively. The most important feature of Fig. 11(b) is that an irregular shaped region shows up in the right-upper corner of Fig. 11(b), indicating the polymer phase formed with a matrix structure of embedded silica nanoparticles.

The TEM-EELS technique was used to distinguish between the thin layer of polymer coating and the hydrophilic silica nanoparticles. Although the wet method used for the coated hydrophobic nanoparticles produced a good dispersion of agglomerated nanoparticles as shown in Fig. 8, we used a dry method for the analysis of the encapsulated hydrophilic silica nanoparticles. In the dry method, a copper grid held by tweezers was ploughed through the coated silica nanoparticles. The very fine agglomerates of nanoparticles become attached to the copper grid due to Van der Waals and electrostatic forces. This sampling method was used to better preserve the integrity of the coated silica nanoparticles.
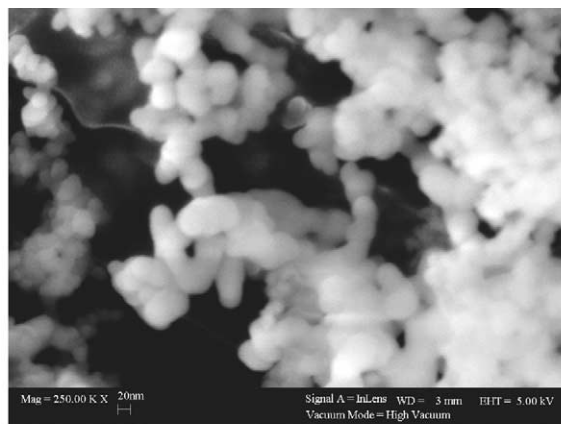
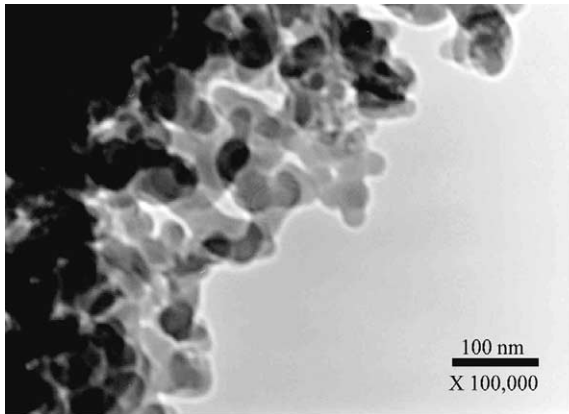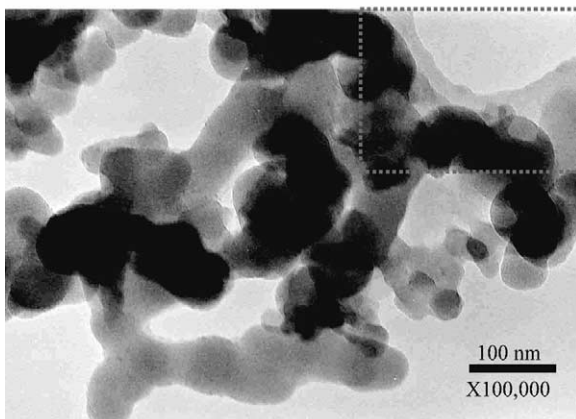Fig. 10. SEM micrographs of hydrophilic silica nanoparticles. (a) Uncoated × 250 000; (b) coated × 200 000.

The Zero-loss micrograph of the agglomerate of coated hydrophilic silica nanoparticles is shown in Fig. 12(a) and the micrographs of silicon and carbon mapping can be found in Fig. 12(b) and (c), respectively. When comparing the regions A and B in Fig. 12(b) and (c), it can be seen that the carbon signal in the carbon mapping micrograph exactly outlines the configuration of the silica nanoparticles shown in the silicon mapping micrograph. From the carbon mapping micrograph, it appears that the hydrophilic silica nanoparticles were also completely encapsulated in a polymer matrix structure.

The hydrophilic silica nanoparticles were also tested using FT-IR, to identify any chemical changes after being coated with the polymer. Fig. 13 shows the

(a)

(b)

Fig. 11. TEM micrographs of hydrophilic silica nanoparticles. (a) Uncoated × 100 000; (b) coated × 100 000.
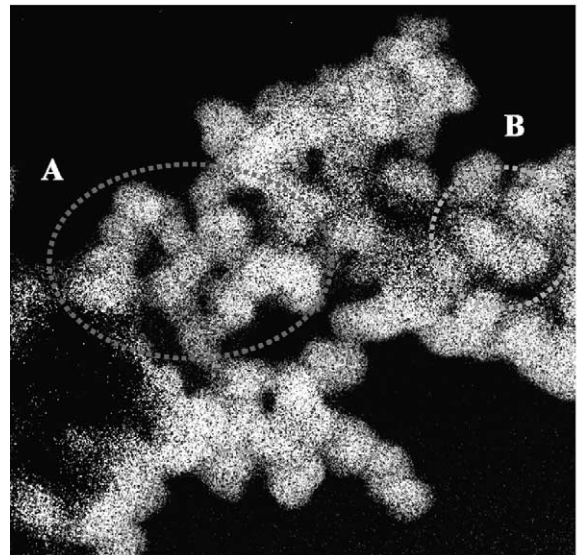
spectra of uncoated silica nanoparticles, coated silica particles, and pure polymer powder, respectively. The results are practically the same as those found for the hydrophobic silica particles, again supporting the observations in the SEM and TEM micrographs (Figs. 11 and 12) that the surface of the hydrophilic silica nanoparticles is coated with polymer in a matrix structure.

The Degussa hydrophobic silica (Aerosil® R972) was manufactured by modifying the surface with dimethyldichlorosilane so that it exhibits a hydrophobic (water-repelling) property. We were somewhat surprised to find that the FT-IR spectra of the uncoated hydrophobic silica (Fig. 9(b)) appears to be exactly the same as that of the uncoated hydrophilic

silica (Fig. 13(b)). The peaks from the methyl groups and from the C–Si bond were not observed in the Fig. 9(b). This is attributed to the very low concentration of methyl groups on the hydrophobic silica, which is below the detection limit of the Spectrum
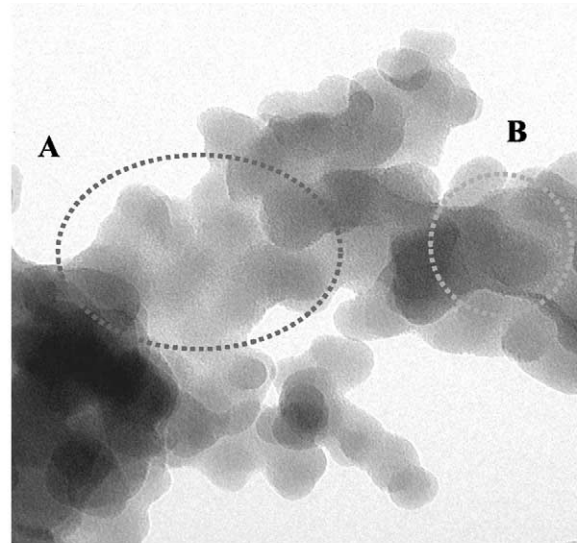
(a)

(b)

Fig. 12. TEM-EELS micrographs of coated hydrophilic nanoparticles. (a) Zero-loss; (b) silicon mapping; (c) carbon mapping.
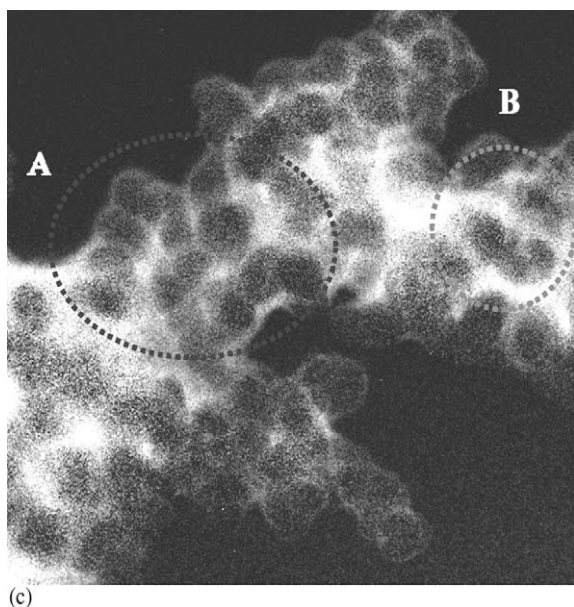
Fig. 12. (*Continued*).

One FT-IR (0.1 wt.%). As observed in Fig. 9(a) and Fig. 13(a), the spectra of the coated hydrophobic and hydrophilic silica also appear to be the same. This result indicates that the SAS coating process is a purely physical deposition of precipitated polymer on the surface of particles and is therefore independent of the hydrophilicity or hydrophobicity of the surface of the silica nanoparticles.

However, the surface coverage of polymer on the hydrophobic silica particles appears to be somewhat less than that of the hydrophilic silica particles when comparing Fig. 8(c) to Fig. 12(c). This is due to the fact that a somewhat larger polymer to silica ratio was used in the hydrophilic coating experiments (Table 2)

4.4. Coating of 600 nm silica nanoparticles

To further evaluate the SAS coating process, experiments to encapsulate 600 nm silica hydrophilic nanoparticles were conducted. The SEM microphotograph in Fig. 14(a) shows the uncoated monodisperse spherical silica particles with a size of about 600 nm from the scale bar. After the SAS coating process, it is observed that silica particles were coated with a polymer film on their surface (Fig. 14(b), (c), (d)) for all three weight ratios of polymer to silica investigated. When a ratio of polymer to nanoparticles (1:4 weight) is used, a composite particle (agglomerate), containing many primary particles, of about 4 μm was formed (Fig. 14(b)). The formation of these large agglomerates could be due to the plasticization of the polymer by CO_2 [19] under high-pressure conditions since the glass transition temperature of the polymer is depressed by SC CO_2 [35]. The agglomerates are
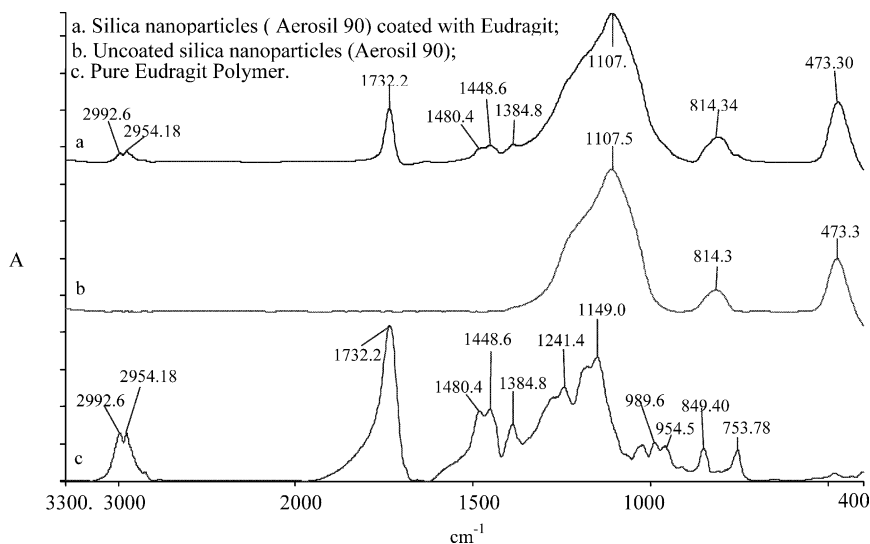

Fig. 13. FT-IR spectra for hydrophilic silica nanoparticles. (a) Coated nanoparticles; (b) uncoated nanoparticles; (c) Eudragit.
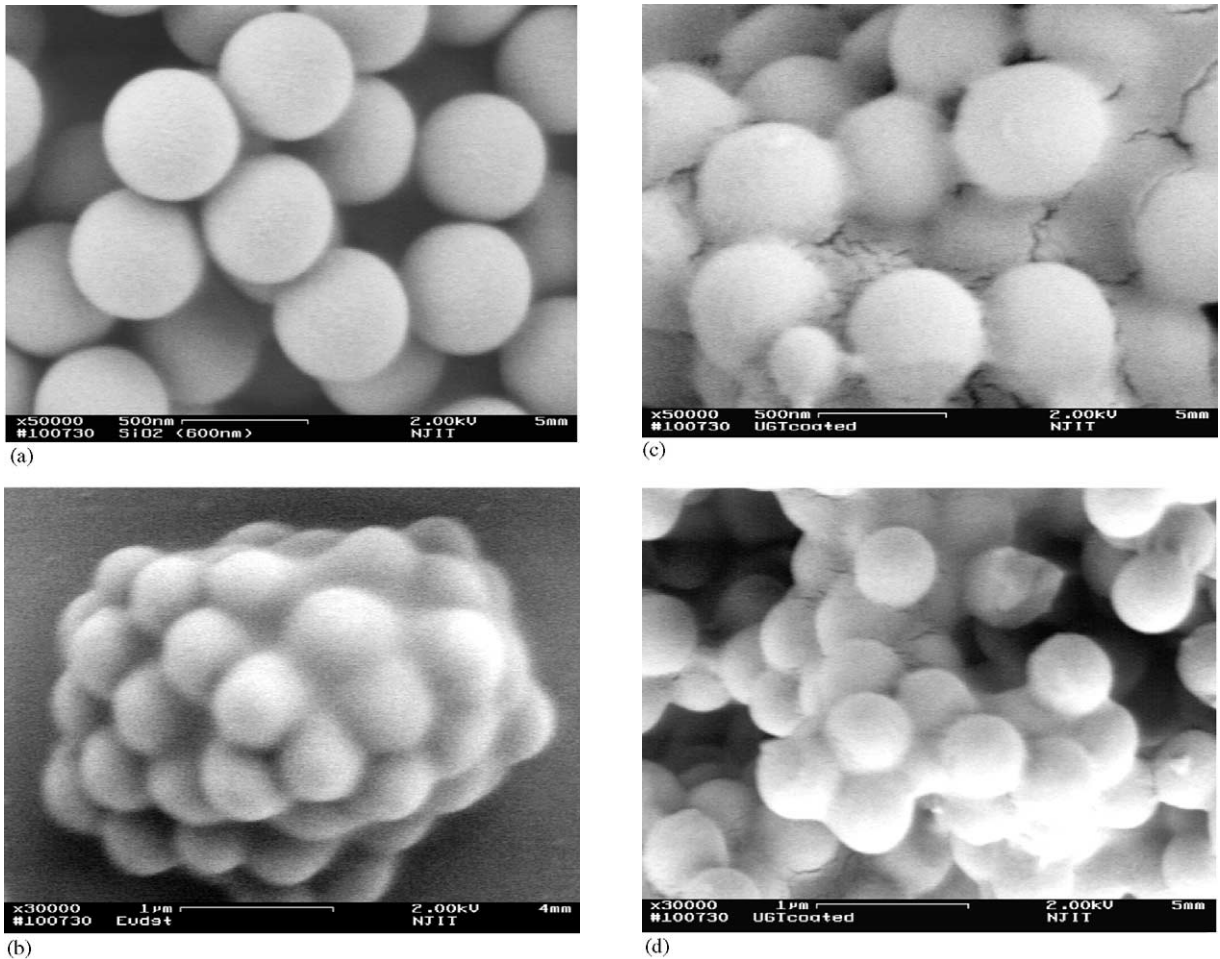
Fig. 14. SEM microphotographs. (a) Uncoated 600 nm silica particles; (b) coated (polymer to silica, 1:4); (c) (1:5); (d) (1:6).

also formed when using a lower ratio of polymer to nanoparticles by weight (Fig. 14(c) and (d)). However, it appears that less agglomeration occurs when less polymer is used.

To estimate the thickness of the coating layer on the surface of the 600 nm particles the Eugragit coated nanoparticles (1:4 weight) were heated in a Perkin Elmer thermo gravimetric analyzer (TGA) to 1073 K to burn off the polymer coating. If it is assumed that the coating forms a spherical layer of constant thickness, h, then

$$h = R\left(1 + \rho_H m_c / \rho_c m_H\right)^{1/3} - R \qquad (1)$$

where R is the radius of the uncoated nanoparticle, ρ_H and ρ_c are the densities of the host nanoparticles
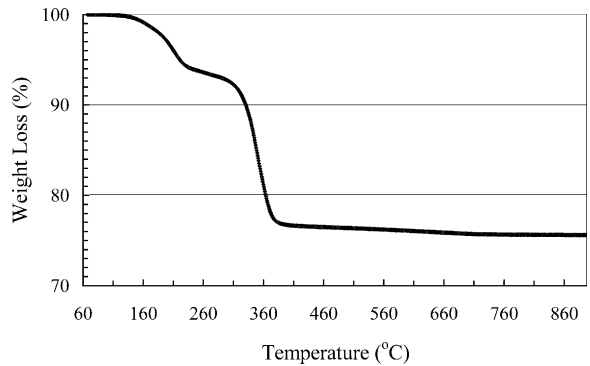

Fig. 15. TGA experiment to estimate the thickness of the coating layer on the surface of 600 nm silica particles coated with Eugragit (1:4).

and polymer coating, respectively and m_H and m_c are the weight of the host and polymer, respectively. From Fig. 15 and Eq. (1), h is estimated to be 75 nm.

5. Concluding remarks

Nanoparticle coating or encapsulation with polymer using the SC CO_2 SAS coating process was investigated in this research. The results revealed that 16–20 nm nanoparticles were successfully coated or encapsulated in polymer by the SAS coating process. The coating or encapsulation of nanoparticles using SC CO_2 SAS coating process appears to be independent of surface hydrophilicity. The mechanism of the SC CO_2 SAS coating process appears to be a heterogeneous polymer nucleation with nanoparticles serving as nuclei with a subsequent growth of polymer on the surface of the nanoparticles induced by mass transfer and phase transition. A polymer matrix structure of encapsulated nanoparticles was formed by agglomeration of the coated nanoparticles. For larger 600 nm particles the thickness of the polymer coating can be controlled by adjusting the ratio of polymer to host particles.

TEM-EELS was found to be the best approach for the characterization of the coated nanoparticles since different elements can be detected at the nanoscale. FT-IR analysis is another valuable qualitative analysis method for material characterization.

The SAS coating process is a promising environmentally friendly technique for nanoparticle coating/encapsulation with polymer with applications to pharmaceuticals and other products where chemical interactions must be avoided.

Acknowledgements

References

[1] A.J. Ruys, Y.W. Mai, The nanoparticle-coating process: a potential sol–gel route to homogeneous nanocomposites, Mater. Sci. Eng. A 265 (1999) 202.

[2] J.X. Zhang, L.Q. Gao, Nanocomposite powders from coating with heterogeneous nucleation processing, Ceram. Int. 27 (2001) 143.

[3] S.Y. Chang, L. Liu, S.A. Asher, Preparation and properties of tailored morphology, monodisperse colloidal silica–cadmium sulfide nanocomposites, J. Am. Chem. Soc. 116 (1994) 6739.

[4] J.C. Leroux, E. Allémann, F.D. Jaeghere, E. Doelker, R. Gurny, Biodegradable nanoparticles—from sustained release formulations to improved site specific drug delivery, J. Control. Rel. 39 (1996) 339.

[5] H. Cohen, R.J. Levy, J. Gao, V. Kousaev, S. Sosnowski, S. Slomkowski, G. Golomb, Sustained delivery and expression of DNA encapsulated in polymeric nanoparticles, Gene Ther. 7 (2000) 1896.

[6] Y. Zhang, Q. Zhang, Y. Li, N. Wang, J. Zhu, Coating of carbon nanotubes with tungsten by physical vapor deposition, Solid State Commun. 115 (2000) 51.

[7] D. Shi, S.X. Wang, W.J. Ooij, L.M. Wang, J.G. Zhao, Z. Yu, Uniform deposition of ultrathin polymer films on the surfaces of Al_2O_3 nanoparticles by a plasma treatment, Appl. Phys. Lett. 78 (2001) 1243.

[8] D. Vollath, D.V. Szabó, Coated nanoparticles: a new way to improved nanocomposites, J. Nanoparticle Res. 1 (1999) 235.

[9] O. Takeo, N. Koichi, S. Katsuaki, Formation of carbon nanocapsules with SiC nanoparticles prepared by polymer pyrolysis, J. Mater. Chem. 8 (1998) 1323.

[10] V.M. Sglavo, R. Dal Maschio, G.D. Soraru, A. Bellosi, Fabrication and characterization of polymer-derived silicon nitride oxide Zirconia (Si_2N_2O–ZrO_2) nanocomposite ceramics, J. Mater. Sci. 28 (1993) 6437.

[11] J.S. Hrkach, M.T. Peracchia, A. Domb, N. Lotan, R. Langer, Nanotechnology for biomaterials engineering: structural characterization of amphiphilic polymeric nanoparticles by ^{1}H NMR spectroscopy, Biomaterials 18 (1997) 27.

[12] D. Wang, D.R. Robinson, G.S. Kwon, J. Samuel, Encapsulation of plasmid DNA in biodegradable poly(D,L-lactic-co-glycolic acid) microspheres as a novel approach for immunogene delivery, J. Control. Rel. 57 (1999) 9.

[13] K.W. Leong, H.-Q. Mao, V.L. Truong-Le, K. Roy, S.M. Walsh, J.T. August, DNA-polycation nanospheres as non-viral gene delivery vehicles, J. Control. Rel. 53 (1998) 183.

[14] Y.S. Jong, J.S. Jacob, K.-P. Yip, G. Gardner, E. Seitelman, M. Whitney, S. Montgomery, E. Mathiowitz, Controlled release of plasmid DNA, J. Control. Rel. 47 (1997) 123.

[15] T.H. Yang, A. Dong, J. Mayer, O.L. Johnson, J.L. Cleland, J.F. Carpenter, Use of infrared spectroscopy to access secondary structure of human growth hormone within biodegradable microsphere, J. Pharm. Sci. 88 (1999) 161.

[16] K. Fu, K. Griebenow, L. Hseih, V.M. Klibanov, R. Langer, FTIR characterization of the secondary structure of proteins encapsulated within PLGA microspheres, J. Control. Rel. 58 (1999) 357.

[17] J.H. Kim, T.E. Paxton, D.L. Tamasko, Microencapsulation of naproxen using rapid expansion of supercritical solutions, Biotechnol. Prog. 12 (1996) 650.

[18] K. Mishima, K. Matsuyama, D. Tanabe, S. Yamauchi, T.J. Young, K.P. Johnston, Microencapsulation of proteins by

rapid expansion of supercritical solution with a nonsolvent, AIChE J. 46 (4) (2000) 857.

[19] M.L. O'Neill, Q. Cao, M. Fang, K.P. Johnston, S.P. Wilkinson, C. Smith, J.L. Kerschner, S.H. Jureller, Solubility of homopolymers and copolymers in carbon dioxide, Ind. Eng. Chem. Res. 37 (1998) 3067.

[20] A. Tsutsumi, S. Nakamoto, T. Mineo, K. Yoshida, A novel fluidized-bed coating of fine particles by rapid expansion of supercritical fluid solutions, Powder Technol. 85 (1995) 275.

[21] T.J. Wang, A. Tsutsumi, H. Hasegawa, T. Mineo, Mechanism of particle coating granulation with RESS process in a fluidized bed, Powder Technol. 118 (2001) 229.

[22] V. Pessey, D. Mateos, F. Weill, F. Cansell, J. Etourneau, B. Chevalier, $SmCo_5/Cu$ particles elaboration using a supercritical fluid process, J. Alloys Compounds 323 (2001) 412.

[23] V. Pessey, R. Garriga, F. Weill, B. Chevalier, J. Etourneau, F. Cansell, Core-shell materials elaboration in supercritical mixture CO_2/ethano, Ind. Eng. Chem. Res. 39 (12) (2000) 4714.

[24] E. Reverchon, G. Della Porta, I. De Rosa, P. Subra, D. Letourneur, Supercritical antisolvent micronization of some biopolymers, J. Supercrit. Fluids 18 (2000) 239.

[25] D.J. Dixon, K.P. Johnston, R.A. Bodmeier, Polymeric materials formed by precipitation with a compressed fluid anti-solvent, AIChE J. 39 (1993) 127.

[26] R. Falk, T.W. Randolph, J.D. Meyer, R.M. Kelly, M.C. Manning, Controlled release of ionic compounds from poly (L-lactide) microspheres produced by precipitation with a compressed antisolvent, J. Control. Release 44 (1997) 77.

[27] T.J. Young, K.P. Johnston, K. Mishima, H. Tanaka, Encapsulation of lysozyme in a biodegradable polymer by precipitation with a vapor-over-liquid antisolvent, J. Pharmaceut. Sci. 88 (1999) 640.

[28] T.W. Randolph, A.J. Randolph, M. Mebes, S. Young, Sub-micrometer-sized biodegradable particles of poly(L-lactic acid) via the gas antisolvent spray precipitation process, Biotechnol. Progress 9 (1993) 429.

[29] C.J. Chang, A.D. Randolph, Solvent expansion and solute solubility predictions in gas-expanded liquids, AIChE J. 36 (1990) 939.

[30] E. Kiran, P.G. Debenedetti, C.J. Peters, Supercritical Fluids: Fundamentals and Applications, NATO Science Series, E 366, Kluwer Academic Publishers, 2000.

[31] C.S. Lengsfeld, J.P. Delplangue, V.H. Barocas, T.W. Randolph, Mechanism governing microparticle morphology during precipitation by a compressed antisolvent: atomization vs. nucleation and growth, J. Phys. Chem. 104 (2000) 2725–2735.

[32] S. Bristow, T. Shekunov, B.Yu. Shekunov, P. York, Analysis of the supersaturation and precipitation process with supercritical CO_2, J. Supercrit. Fluids 21 (2001) 257–271.

[33] J.J. Luo, C. Zhu, R. Dave, and R. Pfeffer, In-Situ Optical Studies on Drop/Practice Formation in Supercritical Fluids, World Congress of Powder Technology, CD-ROM Proceedings, Paper 200, Sydney, Australia, 2002.

[34] E. Reverchon, Supercritical antisolvent precipitation of micro- and nano-particles, J. Supercrit. Fluids 15 (1999) 1.

[35] P.D. Condo, D.R. Paul, K.P. Johnston, Glass transition of polymers with compressed fluid diluents: type II and III behavior, Macromolecules 27 (1994) 365–371.